Partially Melted Zone in Aluminum Welds — Planar and Cellular Solidification

Liquated grain boundaries mostly resolidify with the planar mode but the cellular mode has also been observed

BY C. HUANG AND S. KOU

ABSTRACT. Aluminum Alloy 2219 was gas metal arc welded to study the solidification modes of liquid in the partially melted zone (PMZ), including grain boundary (GB) liquid and liquid spots in the grain interior. GB liquid mostly solidified with the planar solidification mode. The average temperature gradient G across the PMZ was taken as $(T_L–T_E)/w_P$, where T_L is the liquidus temperature, T_E the eutectic temperature and w_P the PMZ width, which was measured with a microscope. The average solidification rate R of the GB liquid was taken as w_L/t_S, where w_L is the thickness of the GB liquid and t_S the solidification time of the GB liquid, which was determined from the measured thermal cycle. The G/R ratio was estimated to be on the order of 10^5°C s/cm², which is close to the minimum G/R required for planar solidification of the alloy. Most GB liquid was too thin to allow enough space for a planar growth front to gradually evolve into a cellular one before solidification was over. Cellular solidification, however, was observed in the PMZ at the bottom of the weld, where G was lowest. It occurred in thicker (15 μm) GB liquid that had to solidify at a higher R and, hence, lower G/R and more room for cellular solidification to develop. Liquid spots away from the weld were smaller and solidified with the planar mode. Near the weld, however, they grew much larger and had to solidify at a much higher R. Both the lower G/R and the larger space for cellular solidification to develop helped break down planar solidification.

Introduction

Extensive liquation can occur in aluminum alloys during welding in a very narrow region immediately outside the fusion zone called the partially melted zone (PMZ) (Ref. 1). Liquation can result in hot cracking during welding (Refs. 1–7) or loss of ductility after welding (Refs. 8–10).

Huang, *et al.* (Refs. 11, 12), recently studied the PMZ in gas metal arc welds of 2219 aluminum alloy, which is essentially a binary Al-Cu alloy with a Cu content between 6 and 7 wt-% Cu. It was observed that extensive liquation occurs both along grain boundaries (GBs) and at large θ (Al_2Cu) particles, which are present in the grain interior and sometimes at GBs as well. The most significant findings are as follows. First, liquation is initiated at the eutectic temperature T_E by the eutectic reaction between the θ phase and the α (Al-rich) matrix to form the liquid eutectic, and is intensified by further melting of the α matrix above T_E. Second, solidification of the GB liquid is directional — upward and toward the weld regardless of the position of the GB relative to the weld. Third, severe Cu segregation occurs both at the GB and in the grain interior, resulting in a Cu-depleted α phase next to a Cu-rich eutectic. The Cu-depleted α either forms a strip along the GB eutectic or surrounds the eutectic particle in the grain interior. Fourth, the PMZ is rather weak and it fractures prematurely under tensile loading; the brittle eutectic fractures badly, while the weak, ductile, Cu-depleted α elongates.

The solidification modes of the liquated material in the PMZ have not been investigated so far. In the present report, the solidification theories for metal casting and crystal growth are applied on a microscopic scale to study solidification in the PMZ. One interesting question to ponder is how a partially melted grain can resolidify with a planar growth front just like a very slowly growing semiconductor crystal (Refs. 13, 14), even though the welding speed is obviously orders of magnitude higher than the crystal growing speed.

KEY WORDS

Aluminum Alloy 2219
Partially Melted Zone
Grain Boundary
Gas Metal Arc Welding
Planar Solidification
Cellular Solidification

Experimental Procedure

Aluminum Alloy 2219 is a commercial, high-strength aluminum alloy, selected because it is a binary Al-Cu alloy with an easy-to-understand solidification. The actual composition of the workpiece is Al-6.79% Cu-0.27% Mn-0.13% Fe-0.12% Zr-0.08% V-0.05% Ti-0.04% Zn-0.01% Si by weight. The dimensions of the workpiece were 20 cm x 10 cm x 7.94 mm. This Cu content, 6.79%, is slightly higher than the 6.33% in the 6.35-mm-thick workpiece used in recent studies (Refs. 11, 12). The workpiece was welded in the as-received condition of T851 in the 20-cm direction. T8 stands for solution heat treating and cold working, followed by artificial aging; T51 stands for stress relieving by stretching (Ref. 15).

Two gas metal arc welds, weld 1 and weld 2, were made perpendicular to the rolling direction under the same welding condition. The welding parameters were 7.20 mm/s (17 in./min) welding speed, 26.5-V arc voltage, 195-A average current and Ar shielding. The welding wire was a 1.2-mm-diameter wire of alloy 2319; the actual composition was Al-6.3% Cu-0.3% Mn-0.18% Zr-0.15% Ti-0.15% Fe-0.10% V-0.10% Si. The wire

C. HUANG and S. KOU are, respectively, Graduate Student and Professor in the Department of Materials Science and Engineering, University of Wisconsin, Madison, Wis.

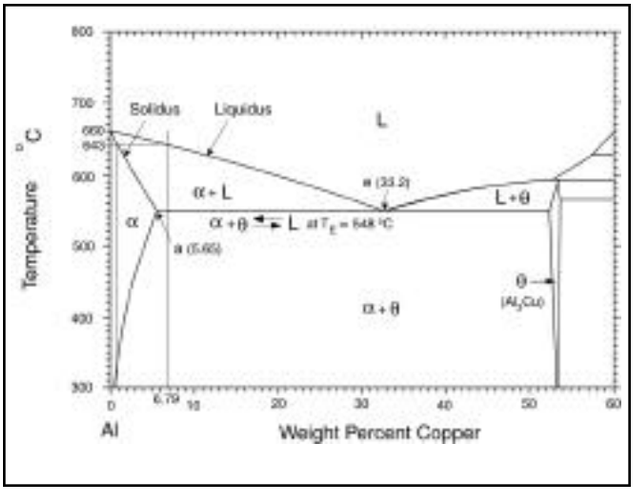

Fig. 1 — Al-Cu phase diagram (Ref. 16).

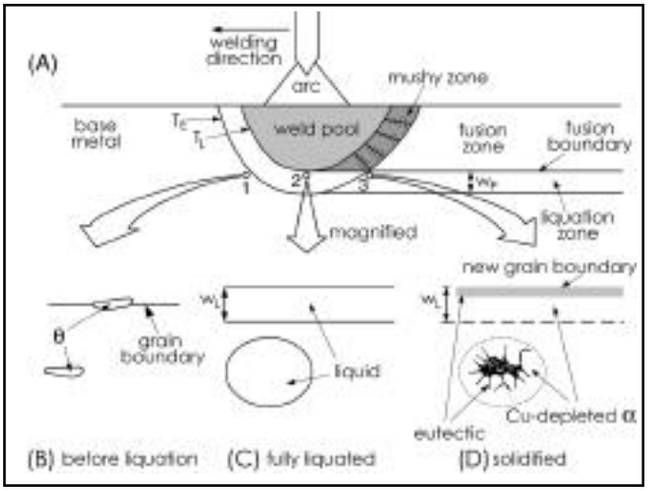

Fig. 2 — Melting and solidification in the partially melted zone: A — Overview; B through D — magnified.

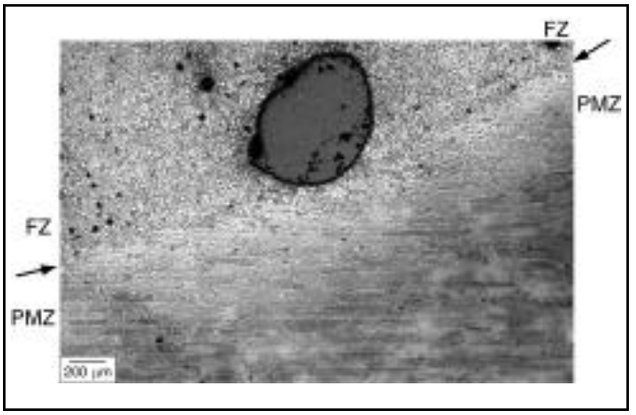

Fig. 3 — Tip of thermocouple sheath in weld 1 at the boundary between the fusion zone (FZ) and the partially melted zone (PMZ). Transverse cross section of weld.

feeding speed was 13.5 cm/s (320 in./min).

An earlier weld, called weld 3 hereafter, was made in the same workpiece and with the same welding wire but under a different set of welding parameters. The welding speed was 12.7 mm/s, the welding voltage was 30 V, the average welding current was 250 A and the wire feeding speed was 18.6 cm/s.

Temperature measurements were initially conducted by inserting thermocouples into holes drilled from the workpiece bottom. However, it was difficult making thermocouples to position at the targeted positions in the PMZ and the heat-affected zone.

Subsequently, temperature measurements were conducted during welding by plunging a thermocouple into the weld pool from behind the arc, at about 45 deg from the vertical plane along the welding direction. This was done with the help of a mechanical device on which the thermocouple was mounted. Only one thermocouple was used in each weld because it was difficult for the device to hold more than one thermocouple at a time and push them to the targeted positions, given the rather limited space between the arc and the trailing pool edge.

The thermocouple was K-type with 0.025-mm-diameter wires and the response time was 0.05 s in air and 0.002 s in water. To protect it from the arc, the thermocouple was inserted in an alumina sheath with a 0.5-mm ID and a 0.15-mm wall. The tip of the sheath was ground thinner to reduce the wall thickness at the tip to less than 0.15 mm. The thermal cycle was recorded with a computer-based data acquisition system.

The resultant welds were etched with a solution of 0.5 vol-% HF in water for optical microscopy.

Results and Discussion

Melting and Solidification in the PMZ

For convenience of discussion, the aluminum-rich portion of the Al-Cu phase diagram is shown in Fig. 1 (Ref. 16). The workpiece is considered here as a binary Al-6.79% Cu alloy as an approximation.

The melting and solidification in the PMZ are shown schematically in Fig. 2. Figure 2A is a vertical cross section of the weld pool and its surroundings that is parallel to the welding direction. Points 1, 2 and 3 are, respectively, located ahead of, inside and behind the region in which liquation is happening. Their corresponding microstructures are shown in Figs. 2B–D.

Large θ particles are present in the grain interior and sometimes at the GB, as shown in Fig. 2B. The liquated material at the GB and in the grain interior is shown in Fig. 2C. Liquation is initiated at the large θ particles at the eutectic temperature T_E by the eutectic reaction between θ and the surrounding α matrix. Liquation is intensified by further melting of the surrounding α at temperatures above T_E.

Point 2 reaches its peak temperature T_L and the width of the GB liquid w_L reaches its maximum when the bottom of the weld pool touches point 2. Solidification of the GB liquid at point 2 begins when the bottom of the weld pool begins to pass point 2 and ends when the eutectic isotherm T_E just passes point 2. The solidification time, t_S, is the same as the residence time of point 2 in the freezing temperature range of T_L to T_E, which can be measured with a thermocouple positioned at the bottom of the weld pool.

The solidification mode of the GB liquid at point 2 depends on the temperature gradient, G, and the solidification rate, R. If the G/R ratio is high enough for planar solidification to occur, the GB liquid will solidify with the planar mode, that is, with a planar solidification front. Solidification occurs from the cooler side of the GB liquid to the warmer. As such, the GB actually shifts toward the weld, as can be seen by comparing the GBs in

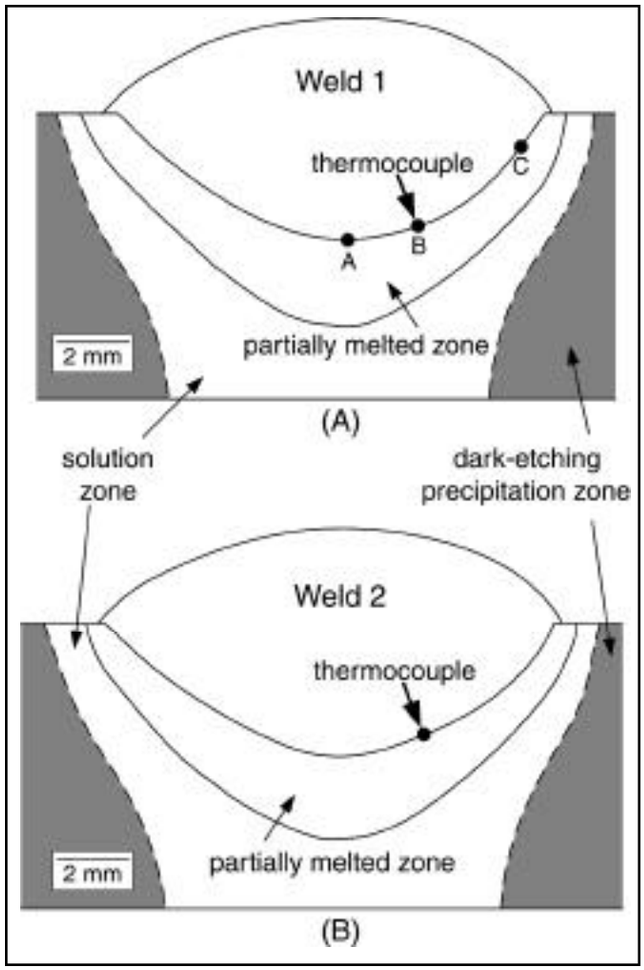

Fig. 4 — Transverse cross sections of partially melted zones: A — Weld 1; B — weld 2. Points A, B and C are locations of the micrographs shown in Figs. 7, 6 and 9, respectively.

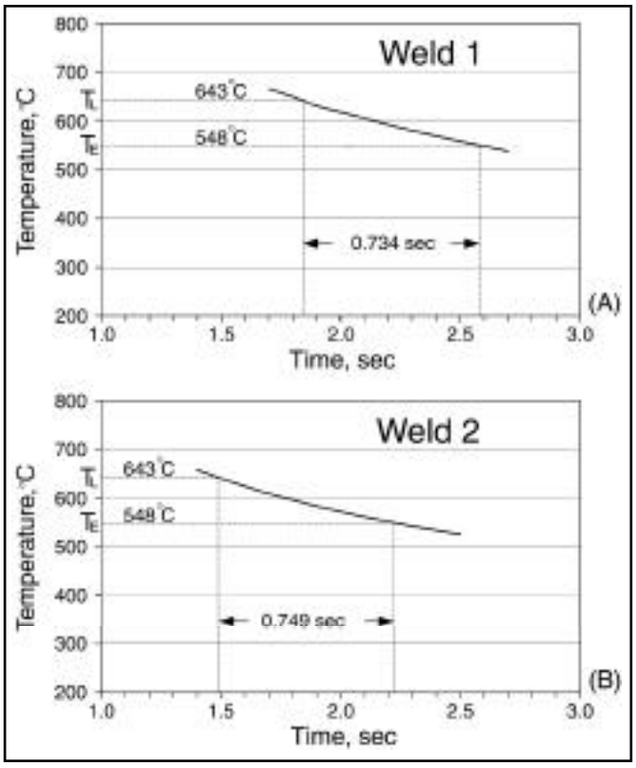

Fig. 5 — Measured thermal cycles showing the solidification times: A — Weld 1; B — weld 2.

Figs. 2B and D. This, in fact, is like Bridgman crystal growth on a microscopic scale. Growth occurs epitaxially from upon the unmelted portion of the grain below the GB liquid, an interesting occurence because the GB liquid in between two neighboring grains is usually thought to solidify from both grains, not just one.

The GB liquid solidifies first as a solute-depleted, eutectic-free material, then as a solute-rich eutectic at the GB. Grain boundary segregation of Cu has been measured and reported in a previous study (Ref. 12).

Width of the PMZ

Figure 3 is a micrograph taken from the transverse cross section of weld 1. It shows the tip of the alumina sheath of the thermocouple plunged into the pool of weld 1. As shown, the thermocouple sheath lands at the fusion boundary. The situation is similar in weld 2.

Figure 4 shows the transverse cross sections of welds 1 and 2 and their PMZs. The upper boundary of the PMZ is the fusion boundary of the weld, that is, T_L = 643°C from the phase diagram — Fig. 1. The lower boundary of the PMZ, that is, T_E = 548°C, needs be determined with the help of a microscope. As shown in previous studies (Refs. 11, 12), the first sign of liquation is observed at the lower boundary of the PMZ, where large θ particles begin to react eutectically with the surrounding α matrix and form solid eutectic upon cooling. The workpiece microstructure is examined under the microscope upward from the bottom surface of the workpiece until these particles are found. This is repeated across the entire weld and its vicinity. The accuracy of the measurements of the distance between T_L and T_E is ±0.04 mm. It should be pointed out that at the location of these particles, GB liquation is usually not yet pronounced enough to be readily recognized because GBs are often free of θ particles (Refs. 11, 12). Therefore, the size of the PMZ can be seriously underestimated if it is measured based on GB liquation.

As shown in Fig. 4, the PMZ is wider at the bottom and narrower on the top. In the vertical direction, the widths of the PMZ in weld 1 are w_P = 2.41 mm at point A, 1.98 mm at point B and 1.76 mm at point C. During welding, the workpiece was free from contact with any materials except at its four corners. As such, the workpiece's bottom surface acts as a thermal barrier to heat flow from the top. This reduces temperature gradients below the weld significantly. The isotherm corresponding to the edge of the dark-etching precipitation zone cuts the workpiece bottom at two separate locations. This is another indication of reduced temperature gradients below the weld. The reduced temperature gradients below a partially penetrating weld have been demonstrated by computer simulation of heat flow during welding (Ref. 17).

Thermal Cycles

Figure 5 shows the thermal cycles measured in welds 1 and 2. The locations of the thermocouples in the welds have been shown previously in Fig. 4. The residence time in the freezing temperature range, that is, from the liquidus tempera-

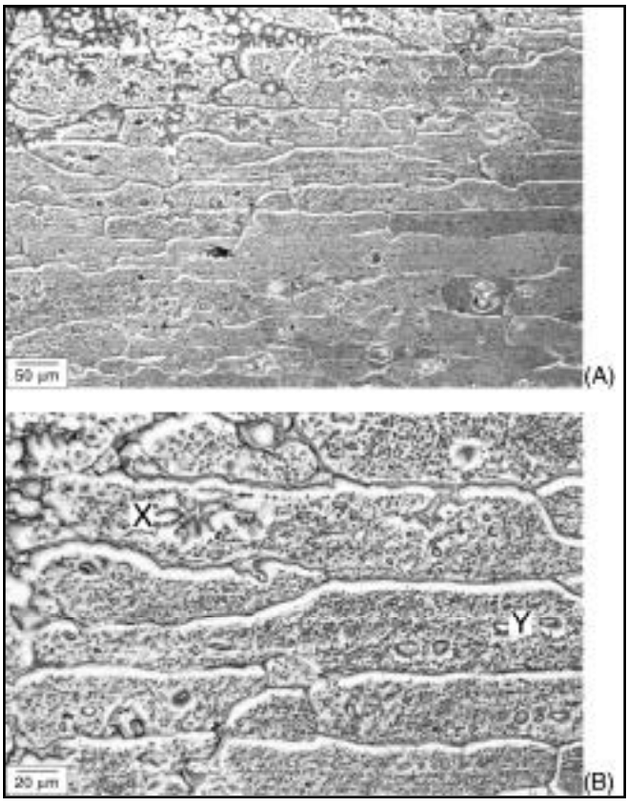

Fig. 6 — Transverse cross section of the microstructure in the partially melted zone at point B in weld 1 (Fig. 4A): A — Lower magnification; B — higher magnification.

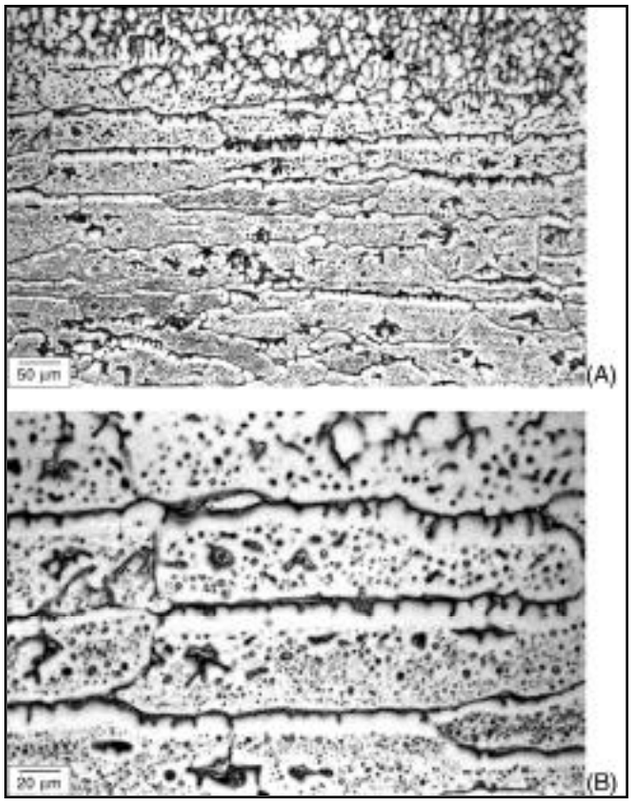

Fig. 7 — Transverse cross section of the microstructure in the partially melted zone at point A of weld 1 (Fig. 4A): A — Lower magnification; B — higher magnification.

ture T_L (643°C) to the eutectic temperature T_E (548°C), will be called the solidification time t_S hereafter. From Fig. 5, t_S = 0.734 s for weld 1 and t_S = 0.749 s for weld 2. These results are close to each other, thus suggesting the validity of the temperature measurement technique.

Solidification Modes of GB Liquid

As already mentioned, the workpiece was welded perpendicular to the rolling direction. In a micrograph on the transverse cross section of the weld, the grains in the PMZ appear elongated in the horizontal direction. As observed in previous studies (Refs. 11, 12), GB liquid tends to solidify upward and toward the weld under the influence of the high-temperature gradient in the PMZ. Since GB liquid is hypoeutectic in composition, it solidifies first as a Cu-depleted α strip and last as the eutectic.

The PMZ microstructure at point B of Fig. 4A is shown in Fig. 6A. The top left corner is in the fusion zone and the rest is in the PMZ. The light-etching strips along the top of the grains in the PMZ are the Cu-depleted α , and the dark-etching GBs at the top of the strips are the eutectic. Some α strips are shown in Fig. 6B at a higher magnification. As shown, the α strips appear to be planar, that is, without cells or dendrites. The PMZ microstructure next to the thermocouple in weld 2 is similar.

The PMZ microstructure at point A of Fig. 4A is shown in Fig. 7A. The fine grain structure at the top is in the fusion zone. The α strip appears to be thicker in some grains and thinner in others. In general, thinner α strips are planar in structure while thicker ones are more likely to be cellular. Some α strips with a cellular structure are shown in Fig. 7B at a higher magnification. The α strips are, on average, significantly thicker than those at point B — Fig. 6B.

The PMZ microstructure near the bottom of weld 3 is shown in Fig. 8A. The 590 J/mm heat input of weld 3 is lower than the 718 J/mm heat input of weld 1. The lower heat input of this weld results in less liquation, and the α strips are on average thinner than those at point A of weld 1 — Fig. 7A. GB solidification is planar everywhere in the PMZ, including at the bottom of the weld (not shown). This is consistent with the lower heat input of weld 3. However, near the sharp turn in the fusion boundary (indicated by the arrow in Fig. 8A), cellular solidification is observed. Some of the cellular α strips are shown in Fig. 8B at a higher magnification. The reason cellular solidification occurs here will be discussed later.

Figure 9A shows the PMZ microstructure near the top of the fusion boundary in weld 1 (point C in Fig. 4A). The upper left corner is part of the weld. The α strips are on average significantly thinner than those in the PMZ at the bottom of the weld (point A in Fig. 4A) shown previously in Fig. 7A. Furthermore, the α strips appear to be planar; no cellular α strips are visible. Some of the planar α strips are shown in Fig. 9B at a higher magnification. It is clear the α strips are either at the top of the grains or along the side of the grains that face the weld. This directional solidification behavior of the GB liquid, *i.e.,* upward and toward the weld, has been previously discussed (Refs. 11, 12).

In order to understand the solidification modes of the GB liquid, the temperature gradient and the growth rate of the GB liquid will be discussed as follows.

G/R Ratio at GB

It is well known in both metal casting and crystal growth (Refs. 13, 14) that

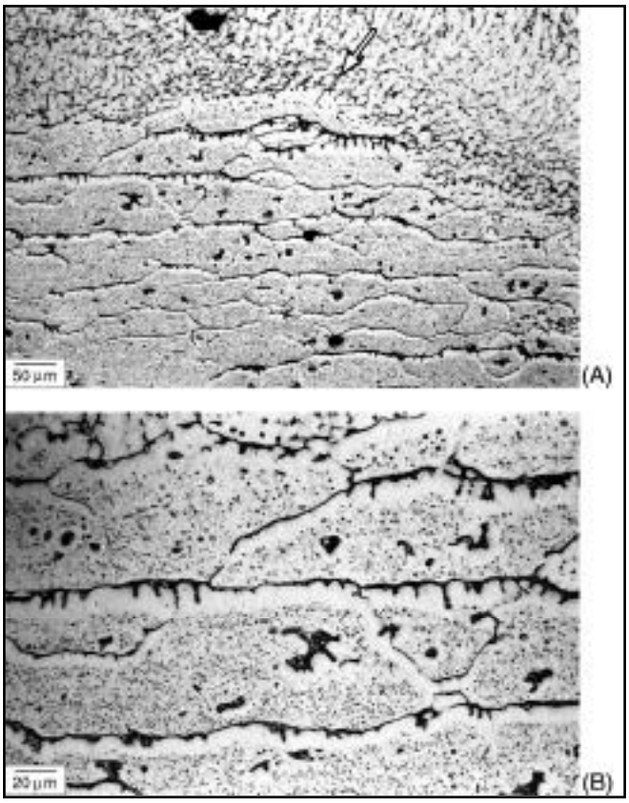

Fig. 8 — Transverse cross section of the microstructure in the partially melted zone at the bottom of weld 3: A — Lower magnification; B — higher magnification. The arrow in A indicates a sharp turn in the fusion boundary.

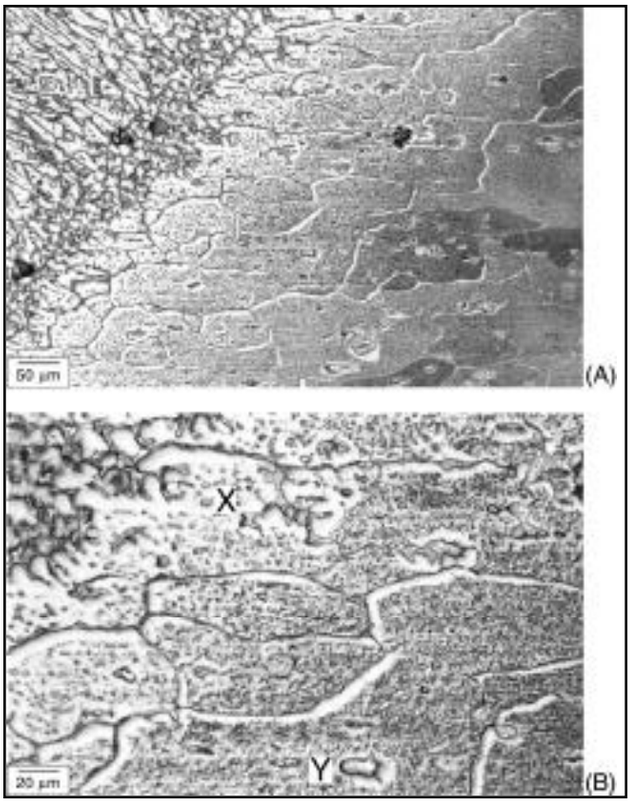

Fig. 9 — Transverse cross section of the microstructure in the partially melted zone at point C of weld 1 (Fig. 4A): A — Lower magnification; B — higher magnification.

temperature gradient G and growth rate R, both in the direction perpendicular to the growth front (the solid/liquid interface), are the two most fundamental parameters of solidification. They determine the solidification mode, which in turn determines the resultant solidification microstructure.

The temperature gradient and the growth rate of GB liquid in the PMZ will be estimated as follows. Consider point 2 in Fig. 2A. As an approximation, the temperature gradient is

$$G \quad \frac{T_L - T_E}{w_P} \qquad (1)$$

where w_P is the width of the PMZ. This G is the average temperature gradient across the width of the PMZ.

Let w_L be the thickness of the GB liquid, as shown in Fig. 2C. As an approximation, the growth rate of the GB liquid is

$$R \quad \frac{w_L}{t_S} \qquad (2)$$

where t_S is the solidification time of the GB liquid. This R is the average growth rate of the GB liquid. From Equations 1 and 2

$$\frac{G}{R} \quad \frac{(T_L - T_E)t_S}{w_P w_L} \qquad (3)$$

According to the constitutional supercooling theory (Refs. 1, 13), for a planar solidification front to be stable, the following criterion must be met:

$$\frac{G}{R} \geq \frac{-m_L C_L (1-k)}{D_L} \qquad (4)$$

where m_L is the slope of the liquidus line in the phase diagram, C_L the solute concentration of liquid at the growth front, k the segregation coefficient and D_L the diffusion coefficient of solute in the liquid. If G/R is less than the right-hand side (RHS) of Equation 4, the planar solidification front will break down into a cellular or dendritic one.

Equations 3 and 4 can be further combined to give the following criterion for plane front solidification of the GB liquid

$$\frac{(T_L - T_E)t_S}{w_P w_L} \geq -\frac{m_L C_L (1-k)}{D_L} \qquad (5)$$

The RHS of Equation 4 can be determined with the help of the phase diagram. As an approximation, the liquidus line and the solidus line of the phase diagram are both assumed to be a straight line. From Fig. 1, the slope of the liquidus line is m_L = (548–660°C)/(33.2–0% Cu) = -3.37°C/% Cu. The equilibrium partition ratio, k = 5.65% Cu/33.2% Cu = 0.17. At the fusion boundary of weld 1, *i.e.*, at the liquidus temperature 643°C, C_L is 6.79% Cu. The diffusion coefficient of Cu in liquid Al-5% Cu is about 5 x 10^{-5} cm^2/s (Ref. 18). From these data, the RHS of Equation 4 becomes the following:

$$-\frac{m_L C_L (1-k)}{D_L}$$

$$= \frac{(3.37°C/\%Cu) \times 6.79\%Cu \times (1-0.17}{5 \times 10^{-5} cm^2/s}$$

$$= 3.80 \times 10^5 \frac{°C\,s}{cm^2} \qquad (6$$

The left-hand side (LHS) of Equation 4, *i.e.*, the G/R ratio, has to be greater than this threshold value if the GB liquid is to have a stable planar solidification front.

To find the G/R ratio, the temperature gradient G and the growth rate R will both have to be determined first. To de-

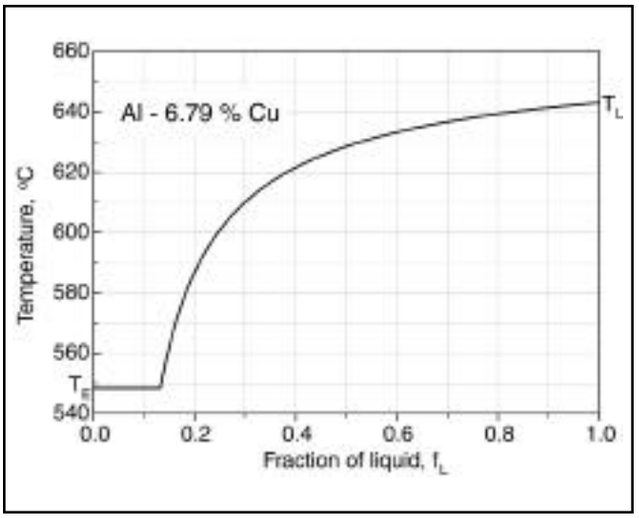

Fig. 10 — Relationship between fraction of liquid and temperature in Al-6.79% Cu.

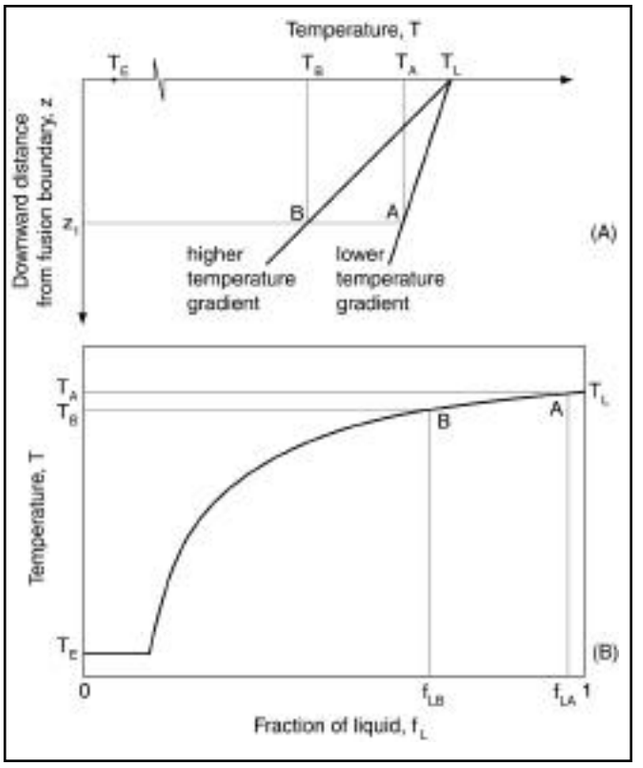

Fig. 11 — Comparison between two points, A and B, located at a very short but equal distance below the fusion boundary: A — Temperature; B — fraction of liquid.

termine the temperature gradient G from Equation 1, the width of the PMZ is needed. Since the GBs are essentially horizontal because of rolling, the GB liquid is essentially horizontal, too. As such, the relevant temperature gradient G should be the one in the vertical direction, *i.e.*, perpendicular to the GB liquid. Therefore, the PMZ width, w_P, is taken as the vertical distance from the fusion boundary (the liquidus temperature T_L) to the location where θ begins to react with the surrounding α matrix eutectically (the eutectic temperature T_E).

Consider point B in Fig. 4A. As already mentioned, at point B in weld 1, w_P = 1.98 mm. From Equation 1 and with T_L = 643°C and T_E = 548°C, the average temperature gradient G perpendicular to the GB liquid at point B is the following:

$$G \quad \frac{T_L - T_E}{w_P} = \frac{643°C - 548°C}{0.198cm} = 480 \frac{°C}{cm} \qquad (7)$$

The average growth rate R perpendicular to the GB liquid can be determined from Equation 2. As already shown, t_S = 0.734 s at point B in weld 1. For an α strip of about 5 μm thick, Equation 2 becomes the following:

$$R = \frac{w_L}{t_S} = \frac{5 \times 10^{-4}\ cm}{0.734\ s} = 6.81 \times 10^{-4} \frac{cm}{s} \qquad (8)$$

From Equations 7 and 8,

$$\frac{G}{R} = \frac{480°C / cm}{6.81 \times 10^{-4} cm / s} = 7.05 \times 10^5 \frac{°C\ s}{cm^2} \qquad (9)$$

This G/R is above the threshold value of 3.80 x 10^5°C s/cm² in Equation 6 for planar solidification. This appears to be consistent with the micrograph in Fig. 6A. The α strips have an average thickness of about 5 μm and they appear planar.

It is worth mentioning, however, that C_L in Equation 6 (the Cu content at the growth front of solidifying GB liquid) is not constant but increases during solidification. Therefore, at some point during solidification, $-m_L C_L(1 - k)/D_L$ can become greater than G/R and planar solidification can break down. From the micrograph in Fig. 6, however, it does not look like this has happened. Discussion of this question follows.

According to the classic theory of interface stability of Mullins and Sekerka (Refs. 19–21), when instability occurs at the planar growth front, it initiates as a perturbation at a certain wavelength. The amplitude of the perturbation can gradually grow and eventually result in a cellular growth front. From Figs. 7B and 8B, the cellular spacing appears to be significantly greater than the width of GB liquid shown in Fig. 6B. This implies that for the GB liquid shown in Fig. 6B, a planar growth front would not seem to have enough space to evolve into a cellular one before solidification is over. This may explain why planar solidification did not break down before GB solidification was over. In fact, this also implies that even with a G/R ratio below the threshold value, cellular solidification may not necessarily occur if the GB liquid is too thin to allow enough room for a planar growth front to gradually evolve into a cellular one before solidification is over.

Consider point C in Fig. 4A, where the width of the PMZ in the vertical direction is 1.76 mm. The temperature gradient perpendicular to the GB liquid is, therefore, G = (643–548°C)/0.176 cm = 540°C/cm, which is higher than the 480°C/cm shown previously in Equation 7. From its micrograph shown in Fig. 9, the average thickness of the α strips is about 5 μm. The solidification time, t_S, is not available. If it is assumed to be close to that at point B (t_S = 0.734 s) as an approximation, the growth rate R = 6.81 x 10^{-4} cm/s and the G/R ratio = 7.93 x 10^5°Cs/cm², which is above the threshold value of 3.80 x 10^5°C s/cm² for planar solidification. This appears to be consistent

with the planar α strips shown in Fig. 9B.

Now consider point A in Fig. 4A, where the width of the PMZ in the vertical direction is 2.41 mm. The temperature gradient perpendicular to the GB liquid is G = (643–548°C)/0.241 cm = 394°C/cm. From its micrograph shown in Fig. 7B, the average thickness of the α strips is almost 15 μm thick. The solidification time, t_S, is not available. Again, if it is assumed to be close to that at point B (t_S = 0.734 s) as an approximation, the growth rate R = 2.04 x 10^{-3} cm/s and the G/R ratio = 1.93 x 10^5°C s/cm^2, which is below the threshold value of 3.80 x 10^5°C s/cm^2 for planar solidification. This appears to be consistent with the cellular GB α strips shown in Fig. 7.

It should be pointed out that considering the uncertainties in D_L and other values in the calculations, the G/R ratios of 1.93 x 10^5°C s/cm^2 for point A, 7.05 x 10^5°C s/cm^2 for point B and 7.93 x 10^5°C s/cm^2 for point C are not really much different from the threshold value of 3.80 x 10^5°C s/cm^2. What is of primary importance, however, is that at points A, B and C of weld 1, the differences in G/R are consistent with the change in the solidification mode of the GB liquid.

Fraction of Liquid and Width of GB Liquid

As previously mentioned, in weld 1 the grain boundary liquid is thicker at point A than at point B, which are about the same distance below the fusion boundary. This can be explained as follows:

Figure 10 shows the relationship between temperature and the fraction of liquid for the Al-6.79% Cu base metal, based on the Scheil equation (Refs. 1, 13). As shown, the fraction of liquid increases rapidly with increasing temperature as the liquidus temperature, T_L, is approached. As already mentioned, the temperature gradient G is significantly (22%) higher at point B than at point A. Therefore, as shown in Fig. 11A, the temperature at point A is higher than that at point B, even though they are at the same distance, z_1, below the fusion boundary. As shown in Fig. 11B, the fraction of liquid at point A can be significantly greater than that at point B because the fraction increases sharply as the liquidus temperature is approached. Since the local average fraction of liquid is higher at point A than at point B, the GB liquid is thicker at point A than at point B.

Since the temperature is higher at point A than at point B, from the phase diagram (Fig. 1) the composition of the GB liquid can be expected to be lower at A than at B. This suggests that, based on Equation 4, the threshold G/R ratio for planar solidification can be lower for point A than for point B, and not exactly fixed at a constant value as suggested by Equation 6. Although this is in favor of planar solidification at point A, cellular solidification can still occur at point A in view of its significantly lower G and higher R.

Figure 11 can also help explain the cellular solidification in weld 3 shown in Fig. 8. As mentioned previously, the 590 J/mm heat input of this weld is lower than the 718 J/mm heat input of weld 1, and GB solidification is planar everywhere in the PMZ except near the arrow shown in Fig. 8A. The temperature gradient G is lower in the area because the material here has to absorb heat coming from two sides, rather than one, and because it has less mass to act as an effective heat sink. According to Fig. 11, the local temperature here is higher and the local fraction of liquid is also higher. Consequently, the width of GB liquid w_L is greater here and, from Equation 2, growth rate R is higher. As such, the lower local G/R ratio here favors cellular solidification. The wider GB liquid also provides more room for cellular solidification to evolve.

Solidification Modes within Grains

In the PMZ, large θ particles present in the grain interior react eutectically with the surrounding α matrix and form liquid spots during welding. One such liquid spot has been shown schematically in Fig. 2C. As the fusion boundary is approached, the size of the liquid spot increases rapidly, *i.e.*, the local average fraction of liquid increases sharply. According to Fig. 10, as the liquidus temperature (fusion boundary) is approached, the fraction of liquid increases sharply.

Particle X in Fig. 6B results from the solidification of a large liquid spot near the weld. In fact, as shown in Fig. 6A, several similar particles are present in the area to the left and above this one. Apparently, the solidification mode is not planar because the morphology of the eutectic in particle X appears complex. With a liquid spot, essentially one half of its perimeter faces the weld, along which directional solidification toward the weld can occur. Since the growth front is concave toward the liquid rather than flat, solute rejected by the growth front can accumulate more rapidly. Perhaps this has helped trigger early breakdown of planar solidification. The liquid spot is much thicker than the GB liquid nearby, *i.e.*, its diameter is several times the width of the GB liquid. This can suggest two things. First, the liquid spot has to solidify with a much greater solidification rate R and, hence, a smaller G/R ratio than the GB liquid. Second, the greater thickness of the liquid spot gives more room for nonplanar solidification to evolve.

Particle Y, which is farther away from the weld, is much smaller than particle X and it shows planar α. According to the phase diagram (Fig. 1), the lower the local temperature, the higher the solute content of the liquid. From Equation 4, the threshold G/R is greater at particle Y than at particle X, and thus planar solidification can break down more easily at particle Y than at particle X. However, the liquid appears to be too thin for cellular solidification to evolve before solidification is over at particle Y. Similar particles are also shown in Fig. 9B.

Conclusions

In the present study on the PMZ in welds of aluminum Alloy 2219, planar and cellular solidification have been observed in the PMZ, both at the GB and in the grain interior. GB liquid tends to solidify with the planar solidification mode. This is because the G/R ratio is high and because the GB liquid is too thin for a planar growth front to evolve into a cellular one before solidification is over. The average temperature gradient G can be estimated from the width and temperature range of the PMZ. From the thickness of GB liquid and thermal cycle measured during welding, the average R can also be estimated. The G/R for the GB liquid in the PMZ near the weld is estimated to be on the order of 10^5°C s/cm^2, which is close to that required for planar solidification of the GB liquid. However, in the PMZ at the bottom of the weld, cellular solidification can occur, especially where the GB liquid is thicker (15 μm) because of lower G and higher R. For a partially penetrating weld like those in the present study, the lowest G in the PMZ appeared to be at the bottom of the weld. The average growth rate R is higher for a thicker GB liquid because it has to solidify faster. As such, the G/R ratio is low for a thicker GB liquid at the bottom of the weld, where cellular solidification is observed. Large prior θ particles in the grain interior liquate and form liquid spots that solidify with a planar mode. However, near the weld, liquid spots become much larger and so does R. The much lower G/R and greater spot size allow planar solidification to break down.

Acknowledgments

This work was supported by the National Science Foundation under Grant No. DMR-9803589. The authors are grateful to Bruce Albrecht and Todd

Holverson of Miller Electric Mfg. Co., Appleton, Wis., for donating the welding equipment and for their technical assistance during the study. They also thank the reviewers for their helpful comments.

References

1. Kou, S. 1987. *Welding Metallurgy*. New York, N.Y.: John Wiley and Sons. pp. 29–59, 137–139 and 239–262.

2. Robinson, I. B. 1978. *The Metallurgy of Aluminum Welding.* Pleasanton, Calif.: Kaiser Aluminum Corp.

3. Gittos, N. F., and Scott, M. H. 1981. Heat-affected zone cracking of Al-Mg-Si alloys. *Welding Journal* 60(6): 95-s to 103-s.

4. Dudas, J. H., and Collins, F. R. 1966. Preventing weld cracks in high-strength aluminum alloys. *Welding Journal* 45: 3–11.

5. Lippold, J. C., Nippes, E. F., and Savage, W. F. 1977. An investigation of hot cracking in 5083-0 aluminum alloy weldments. *Welding Journal* 56(6): 171-s to 178-s.

6. Metzger, G. E. 1967. Some mechanical properties of welds in 6061 aluminum alloy sheet. *Welding Journal* 46(10): 457-s to 469-s.

7. Steenbergen, J. E., and Thornton, H. R. 1970. Quantitative determination of the conditions for hot cracking during welding for aluminum alloys. *Welding Journal* 49(2): 61-s to 68-s.

8. Gibbs, F. E. 1966. Development of filler metals for welding Al-Zn-Mg Alloy 7039. *Welding Journal* 45(10): 445-s to 453-s.

9. Young, J. G. 1968. BWRA experience in the welding of aluminum-zinc-magnesium alloys. *Welding Journal* 47(10): 451-s to 461-s.

10. Arthur, J. B. 1955. Fusion welding of 24S-T3 aluminum alloy. *Welding Journal* 34: 558-s to 569-s.

11. Huang, C., and Kou, S. 2000. Partially melted zone in aluminum welds — Liquation mechanism and directional solidification. *Welding Journal* 79(5): 113-s to 120-s.

12. Huang, C., and Kou, S. 2001. Partially melted zone in aluminum welds — Solute segregation and mechanical behavior. *Welding Journal* 80(1): 9-s to 17-s.

13. Flemings, M. C. 1974. *Solidification Processing*. New York, N.Y.: McGraw-Hill. pp. 31–92, 95.

14. Kou, S. 1996. *Transport Phenomena and Materials Processing*. New York, N.Y.: John Wiley and Sons. pp. 526–585.

15. The Aluminum Association. 1982. *Aluminum Standards and Data*. Washington, D. C.: The Aluminum Association. p. 15.

16. American Society for Metals. 1986. *Binary Alloy Phase Diagrams*. Vol. 1. Metals Park, Ohio: American Society for Metals. p. 106.

17. Kou, S., and Le, Y. 1983. Three-dimensional heat flow and solidification during autogenous GTA welding of aluminum plates. *Metallurgical Transactions* 14A: 2245–2253.

18. Ejima, T., *et al.* 1980. Impurity diffusion of fourth period solutes (iron, cobalt, nickel, copper and gallium) and homovalent solutes (indium and thallium) into molten aluminum. *J. Jan. Inst. Met.* 44(3): 316–323.

19. Mullins, W. W., and Sekerka, R. F. 1963. Morphological stability of a particle growing by diffusion or heat flow. *Journal of Applied Physics* 34(2): 323–329.

20. Mullins, W. W., and Sekerka, R. F. 1964. Stability of a planar interface during solidification of a dilute binary alloy. *Journal of Applied Physics* 35(2): 444–451.

21. Sekerka, R. F. 1965. A stability function for explicit evaluation of the Mullins-Sekerka interface stability criterion. *Journal of Applied Physics* 36(1): 264–268.